Available online at www.sciencedirect.com
ScienceDirect
International Journal of Heat and Mass Transfer 51 (2008) 3103–3112
International Journal of HEAT and MASS TRANSFER
www.elsevier.com/locate/ijhmt

Meshless method based on the local weak-forms for steady-state heat conduction problems

Wu Xue-Hong, Tao Wen-Quan *

State Key Laboratory of Multiphase Flow in Power Engineering, School of Energy and Power Engineering, Xi'an Jiaotong University, Xi'an, Shaanxi 710049, PR China

Received 23 March 2007; received in revised form 22 August 2007
Available online 23 October 2007

Abstract

In this article, the meshless local Petrov–Galerkin (MLPG) method is applied to compute two steady-state heat conduction problems of irregular complex domain in 2D space. The essential boundary condition is enforced by the transformation method, and the MLS method is used for interpolation schemes. A numerical example that has analytical solution shows the present method can obtain desired accuracy and efficiency. Two cases in engineering with irregular boundary are computed to validate the approach by comparing the present method with the finite volume method (FVM) solutions obtained from a commercial CFD package FLUENT 6.3. The results show that the present method is in good agreement with FVM. It is expected that MLPG method (which is a truly meshless) is very promising in solving engineering heat conduction problems within irregular domains.

Keywords: Meshless method; Local Petrov–Galerkin method; MLS; Heat conduction

1. Introduction

The finite volume method (FVM) and finite element method (FEM) have been widely applied to solve the practical engineering problems. It is well-known that these methods depend strongly on the mesh properties. However, to compute problems with irregular complex geometries by using these methods, mesh generation is a far more time-consuming and expensive task than solution of the partial differential equations (PDEs), particularly in 3D cases. Owing to the difficulty of FVM and FEM in the mesh generation, a new numerical method, meshless method (also called meshfree method), has been developed fast in the recent years. In the following a brief review is presented. The smoothed particle hydrodynamics method that was initially used for modelling astrophysical phenomena is now widely used in such complicated phenomena as explosion and underwater shock problems [1]. The earlier research works on SPH may be found in Lucy [2] and Monaghan [3]. Diffuse approximation method (DAM) [4] is closely related to the moving least-squares method, which has been used in the framework of a Galerkin formulation to develop the diffuse element method (DEM) [5]. The element free Galerkin (EFG) method [6] is based on the DEM and widely used in many mechanics problems. The reproducing kernel particle method (RKPM) [7] is to improve the SPH approximation to satisfy consistency requirements using a corrections function, and it has been used in nonlinear and large deformation problems of solid mechanics. It should be noted that most of these methods are not really meshless method, since they need to use a background mesh for the numerical integration. The finite point method (FPM) [8] and MLPG method [9,10] are both truly meshless methods. The FPM uses a non-element interpolation scheme-weighted least square and has no integration required. But this method is based on the point collocation, and the solution results are very sensitive to the selection of the collocation points. The MLPG is based

* Corresponding author. Tel.: +86 29 82669106; fax: +86 29 82669738.
E-mail address: wqtao@mail.xjtu.edu.cn (W.-Q. Tao).

0017-9310/$ - see front matter © 2007 Published by Elsevier Ltd.
doi:10.1016/j.ijheatmasstransfer.2007.08.021

Nomenclature

$a(x)$, $\mathbf{a}(\mathbf{x})$	coefficient of basis function and its vector form
h	heat transfer coefficient
n	unit normal vector outward to the boundary
$p(x)$, $\mathbf{p}(\mathbf{x})$	basis function and its vector form
q	heat flux on the boundary
r	size of support for the weight functions
T	temperature
$T^h(x_I)$	trial functions
$\widehat{T}^I$	fictitious nodal values
$w_I(x)$	weight function
x, y	spacial coordinates

Greek symbols

λ	thermal conductivity
$\phi(x)$, $\mathbf{\Phi}(\mathbf{x})$	shape function and its vector form
$\dot{\Phi}$	heat source
Γ_1, Γ_2, Γ_2	boundaries
Ω	problem domain

Subscripts and superscripts

a	analytical
h	approximate
I, J, K	node indices
m	number of terms
M	total number of nodes
N	number of nodes
num	numerical

on the weak form computed over a local sub-domain and easy to deal with different boundary value problems. Detailed introductions of the MLPG method can be found in Atluri and Shen [11].

A number of meshless methods have been developed by different authors to solve heat transfer and fluid flow problems [12–15]. The focus of the present study is concentrated on the heat conduction problems. In the following a brief review related to the present study is presented. Cleary and Monaghan [16] and Chen et al. [17] employed smoothed particle hydrodynamics method to solve unsteady-state heat conduction problem. Singh and his colleagues used EFG method to solve a number of heat conduction problems, including the nonlinear heat conduction [18], 2D fins [19], 3D steady-state [20] and transient [21] heat conduction problems and composite heat transfer problems [22],and their investigated results show that the EFG results are more accurate than the FEM results [18]. Liu et al. [23] used meshless weighted least-squares (MWLS) method to solve steady- and unsteady-state heat conduction problems. Tan et al. [24] applied least-squares collocation meshless method to solve coupled radiative and heat conduction problems. Sadat et al. [25] used DAM to solve a two-dimensional heterogeneous heat conduction problem. Qian et al. [26] applied MLPG method to compute three-dimensional transient heat conduction problem. Sladek et al. [27,28] applied MLPG method to solve the heat conduction problem in an anisotropic medium.

From above brief review on meshless method application in solving heat conduction problems, we can see that previous researchers have focused mainly on using EFG, SPH and MLPG method. However, the EFG method needs a background mesh for the integrals in the weak form, hence it is not really meshless method; the SPH and DAM and MLWS method are built on the collocation point schemes, for which the selection of the collocation point are important, and the numerical accuracy goes down near the boundary. MLPG method is a truly meshless method; it offers a lot of flexibility to deal with problems of different boundary conditions. A wide range of problems have been investigated by Atluri and his coauthors using MLPG method. Almost all of the previous works limited to heat conduction problems of regular domain. However, many problems in engineering are in irregular domain, and FVM and FEM are difficult to describe accurately boundaries of the irregular domain unless the mesh is very fine, or special grid generation method is adopted which is usually time-consuming. Meshless methods can overcome this difficulty because they do not need mesh. Meshless methods distribute arbitrarily scattering points in the problem domain, so they will have more advantages in solving problems with irregular domain than FVM and FEM. So in the present paper, we apply MLPG method to compute two steady-state heat conduction problems of irregular domain encountered in engineering.

The following discussion begins with implementation of local Petrov–Galerkin method for heat conduction problem in Section 2. The results of numerical examples and discussion are presented in Section 3. The paper ends with conclusions in Section 4.

2. Implementation of local Petrov–Galerkin method for heat conduction problem

As other numerical simulation methods such as FVM, the MLPG method needs some kind of interpolation schemes and discretization methods to generate the algebraic equations, which can be solved numerically. There are a number of local interpolation schemes, such as moving least-square (MLS) approximation, partition of unity

method (PUM), Shepard function, reproducing kernel particle method (RKPM), etc. The MLS is selected in the present paper.

2.1. The moving least-square approximation scheme

The MLS approximation is now widely used in meshless methods for interpolation schemes. The MLS approximation consists of three components: a basis function, a weight function associated with each node, and a set of coefficients that depends on node position.

Consider a sub-domain Ω_X, which is located within the problem domain Ω (see Fig. 1) and has a number of randomly located nodes x_I ($I = 1,\ldots,N$). The moving least squares approximate $T^h(x)$ of $T(x)$ by following definition:

$$T^h(x) = \sum_{i=1}^{m} p(x)a(x) = \mathbf{p}^{\mathrm{T}}(\mathbf{x})\mathbf{a}(\mathbf{x}) \tag{1}$$

where $\mathbf{p}^{\mathrm{T}}(\mathbf{x}) = [p_1(x), p_2(x), \ldots, p_m(x)]$ is a complete monomial basis, m is the number of terms in the basis, and $\mathbf{a}(\mathbf{x}) = [a_1(x), a_2(x), \ldots, a_m(x)]$ is the corresponding coefficient. For example, for a 2D problem, the basis can be chosen as

$$\begin{aligned} &\text{Linear basis}: \mathbf{p}^{\mathrm{T}}(\mathbf{x}) = [1, x, y], \quad m = 3 \\ &\text{Quadratic basis}: \mathbf{p}^{\mathrm{T}}(\mathbf{x}) = [1, x, y, x^2, xy, y^2], \quad m = 6 \end{aligned} \tag{2}$$

The coefficient vector $\mathbf{a}(\mathbf{x})$ is determined by minimizing the difference between the local approximation and the function, and is defined as

$$\begin{aligned} J(\mathbf{a}(\mathbf{x})) &= \sum_{I=1}^{N} w_I(x)[T^h(x_I) - \widehat{T}^I]^2 \\ &= \sum_{I=1}^{N} w_I(x)[\mathbf{p}^{\mathrm{T}}(\mathbf{x}_I)\mathbf{a}(\mathbf{x}) - \widehat{T}^I]^2 \\ &= [\mathbf{p}\cdot\mathbf{a}(\mathbf{x}) - \widehat{\mathbf{T}}]\cdot\mathbf{W}\cdot[\mathbf{p}\cdot\mathbf{a}(\mathbf{x}) - \widehat{\mathbf{T}}] \end{aligned} \tag{3}$$

where x_I denotes the position vector of node I; $w_I(x)$ is the weight function associated with the node I; N is the number of node in Ω_X for which the weight functions $w_I(x) > 0$ are searched; and the matrices $\mathbf{P}$ and $\mathbf{W}$ are defined as

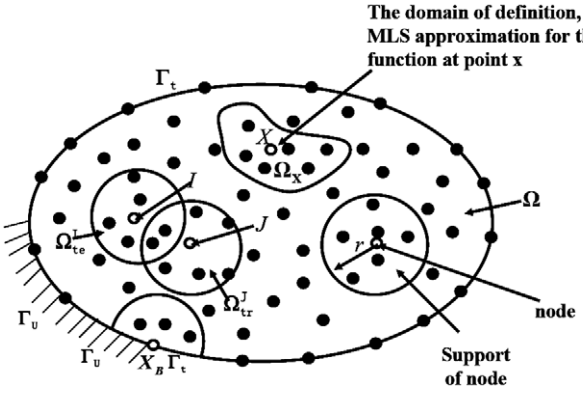

Fig. 1. Schematics of the MLS approximation.

$$\mathbf{P} = \begin{bmatrix} 1 & x_1 & y_1 & \cdots & p_m(x_1) \\ 1 & x_2 & y_2 & \cdots & p_m(x_2) \\ \vdots & \vdots & \vdots & \vdots & \vdots \\ 1 & x_N & y_N & \cdots & p_m(x_N) \end{bmatrix} \tag{4}$$

$$\mathbf{W} = \begin{bmatrix} w_1(x) & \cdots & 0 \\ \vdots & \ddots & \vdots \\ 0 & \cdots & w_N(x) \end{bmatrix} \tag{5}$$

and

$$\widehat{\mathbf{T}}^{\mathrm{T}} = [\widehat{T}^1, \widehat{T}^2, \ldots, \widehat{T}^N] \tag{6}$$

In Eq. (6) $\widehat{T}^I$ is the fictitious nodal value. It is not the nodal value of trial functions denoted by $T^h(x)$. Fig. 2 gives a simple case for the distinction between $\widehat{T}^I$ and $T^h(x)$.

To find the coefficient $\mathbf{a}(\mathbf{x})$, we obtain the extremum by

$$\frac{\partial J(\mathbf{a}(\mathbf{x}))}{\partial(\mathbf{a}(\mathbf{x}))} = 2\sum_{I=1}^{N} w_I(x)\left[\sum_{i=1}^{m} p_i(x_I)a(x) - \widehat{T}^I\right]p_i(x_I) = 0 \tag{7}$$

This leads to the following set of linear relations:

$$\mathbf{A}(\mathbf{x})\mathbf{a}(\mathbf{x}) = \mathbf{B}(\mathbf{x})\widehat{\mathbf{T}} \tag{8}$$

where the matrices $\mathbf{A}(\mathbf{x})$ and $\mathbf{B}(\mathbf{x})$ are defined by

$$\mathbf{A}(\mathbf{x}) = \mathbf{P}^{\mathrm{T}}\mathbf{W}\mathbf{P} = \mathbf{B}(\mathbf{x})\mathbf{P} = \sum_{I=1}^{N} w_I(x)\mathbf{p}(\mathbf{x_I})\mathbf{p}^{\mathrm{T}}(\mathbf{x_I}) \tag{9}$$

$$\mathbf{B}(\mathbf{x}) = \mathbf{p}^{\mathrm{T}}\mathbf{w} = [w_1(x)\mathbf{p}(\mathbf{x_2}), w_2(x)\mathbf{p}(\mathbf{x_2}), \ldots, w_N(x)\mathbf{p}(\mathbf{x_3})] \tag{10}$$

Solving $\mathbf{a}(\mathbf{x})$ from Eq. (8), and substituting it into Eq. (1), we can obtain the final form of the MLS approximation as

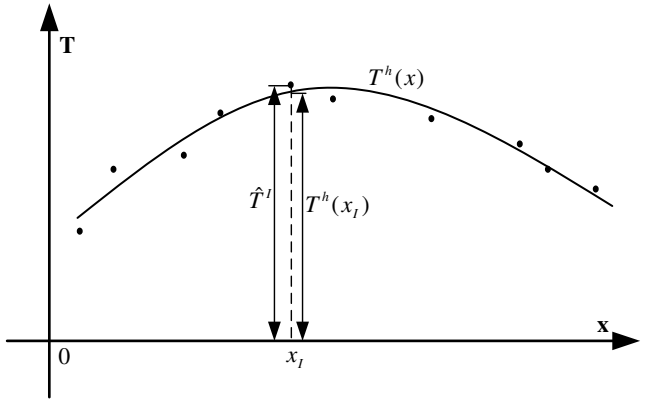

Fig. 2. The approximate function $T^h(x)$ and the nodal parameters T^I in the MLS approximation.

$$T^h(x) = \mathbf{\Phi^T}(\mathbf{x}) \cdot \widehat{\mathbf{T}} = \sum_{I=1}^{N} \phi(x)\widehat{T}^I, \quad x \in \Omega_X \tag{11}$$

where $\mathbf{\Phi^T}(\mathbf{x}) = \mathbf{p^T}(\mathbf{x})\mathbf{A^{-1}}(\mathbf{x})\mathbf{B}(\mathbf{x})$ is the shape function, and its partial derivatives are obtained from Eq. (11)

$$\phi^I_{,k} = \sum_{j=1}^{m}[p_{j,k}(\mathbf{A^{-1}B})_{jI} + p_j(\mathbf{A^{-1}B}_{,k} + \mathbf{A}^{-1}_{,k}\mathbf{B})_{jI}] \tag{12}$$

In Eq. (12) $\mathbf{A}^{-1}_{,k} = (\mathbf{A^{-1}})_{,k}(k = (x, y, z))$, it represents the derivative of the inverse of $\mathbf{A}$, which is given by

$$\mathbf{A}^{-1}_{,k} = -\mathbf{A^{-1}A}_{,k}\mathbf{A^{-1}} \tag{13}$$

2.2. The weight function

In practical applications, the weight function $w_I(x)$ is generally nonzero over the small neighborhood of point x_I, and this neighborhood is called the domain of influence of node I (see Fig. 1). Typically, the shape of the domain in the two-dimensional space can be circular, ellipse, rectangular or any other convenient regular closed lines and in the three-dimensional space can be sphere, ellipsoid, cube or any other simple cubic volume. In the present analysis a circular domain has been selected. The choice of weight function $w_I(x)$ affects the resulting approximation $T^h(x)$, therefore, its selection is of essential importance. Numerical practices of [9,22] have shown that a quadratic spline weight function works well. Hence in this article, the quadratic spline weight function is used. Thus we have

$$w_I(x) = \begin{cases} 1 - 6D_I^2 + 8D_I^3 - 3D_I^4, & 0 \leqslant D_{\mathrm{I}} \leqslant 1 \\ 0, & D_{\mathrm{I}} > 1 \end{cases} \tag{14}$$

where $D_I = \sqrt{(x - x_I)^2 + (y - y_I)^2}/r$, and r is the size of support (see Fig. 1) for the weight functions. It can be seen that the quadratic spline weight function is C^1 continuous over the entire domain.

2.3. Enforcement of essential (Dirichlet) boundary conditions

In MLPG shape functions do not satisfy the Kronecker delta property, and hence when such trial functions are used, it is not easy to implement the essential boundary. Various numerical techniques have been proposed to enforce the essential boundary conditions, such as the Lagrange multiplier method [29], the penalty approach [30], the transformation method [11,31], the direct interpolation method [32], etc. In the present work, the transformation method has been used to enforce essential boundary condition, and the details for implementation of the transformation method can be found in Atluri and coworkers [11,31].

2.4. Numerical implementation for heat conduction problem

The steady-state heat conduction Poisson' equation and boundary conditions can be written as

$$\lambda\frac{\mathrm{d}^2T}{\mathrm{d}x^2} + \lambda\frac{\mathrm{d}^2T}{\mathrm{d}y^2} = \dot{\Phi} \text{ in } \Omega \tag{15}$$

The Dirichlet boundary condition:

$$T = T_1 \text{ on } \Gamma_1 \tag{16}$$

The Neumann boundary condition:

$$-\lambda\left(\frac{\mathrm{d}T}{\mathrm{d}x} + \frac{\mathrm{d}T}{\mathrm{d}y}\right)n_j = q \text{ on } \Gamma_2 \tag{17}$$

The Robin boundary condition:

$$\lambda\left(\frac{\mathrm{d}T}{\mathrm{d}x} + \frac{\mathrm{d}T}{\mathrm{d}y}\right)n_j = h(T_f - T) \text{ on } \Gamma_3 \tag{18}$$

where T represents temperature; λ the thermal conductivity, n_j the outward unit vector to Γ, q the given heat flux, h the convection heat transfer coefficient, T_f is the environmental temperature, $\dot{\Phi}$ the heat source per unit mass, and Γ_1, Γ_2 and Γ_3 the boundaries at which the Dirichlet, Neumann and Robin conditions apply, respectively.

In the Ω_X, the weighted integral form of Eq. (15) is given as

$$\int_{\Omega_x} \lambda\left[\left(\frac{\mathrm{d}^2T}{\mathrm{d}x^2} + \frac{\mathrm{d}^2T}{\mathrm{d}y^2}\right) - \dot{\Phi}\right]w\,\mathrm{d}\Omega_x = 0 \tag{19}$$

To reduce this high-order differentiability requirement on T, we can integrate Eq. (19) by parts. By using Gauss' theorem, we can obtain the following local weak formulation equation:

$$\int_{\Omega_x}\left(\lambda\frac{\mathrm{d}T}{\mathrm{d}x}\frac{\mathrm{d}w}{\mathrm{d}x} + \lambda\frac{\mathrm{d}T}{\mathrm{d}y}\frac{\mathrm{d}w}{\mathrm{d}y} + \dot{\Phi}w\right)\mathrm{d}\Omega_x - \int_{\Gamma}\lambda\left(\frac{\mathrm{d}T}{\mathrm{d}x} + \frac{\mathrm{d}T}{\mathrm{d}y}\right)n_j w\,\mathrm{d}\Gamma = 0 \tag{20}$$

Substituting Eqs. (17) and (18) into Eq. (20), we can obtain following equation:

$$\int_{\Omega_x}\left(\lambda\frac{\mathrm{d}T}{\mathrm{d}x}\frac{\mathrm{d}w}{\mathrm{d}x} + \lambda\frac{\mathrm{d}T}{\mathrm{d}y}\frac{\mathrm{d}w}{\mathrm{d}y} + \dot{\Phi}w\right)d\Omega_x + \int_{\Gamma_2} qw\,\mathrm{d}\Gamma_2 - \int_{\Gamma_3} h(T_f - T)w\,\mathrm{d}\Gamma_3 - \int_{\Gamma_1}\lambda\left(\frac{\mathrm{d}T}{\mathrm{d}x} + \frac{\mathrm{d}T}{\mathrm{d}y}\right)n_j w\,\mathrm{d}\Gamma = 0 \tag{21}$$

The MLS approximation function is given by

$$T = \sum_{I=1}^{N} \Phi_I \cdot \widehat{T}_I \tag{22}$$

Substitution of Eq. (22) into Eq. (21) for all the nodes, we can obtain the following linear equations:

$$\sum_{J=1}^{M}\int_{\Omega_x}\left(\lambda\frac{\mathrm{d}\Phi^J\widehat{T}^J}{\mathrm{d}x}\frac{\mathrm{d}w_I}{\mathrm{d}x}+\lambda\frac{\mathrm{d}\Phi^J\widehat{T}^J}{\mathrm{d}y}\frac{\mathrm{d}w_I}{\mathrm{d}y}\right)\mathrm{d}\Omega_x + \sum_{J=1}^{M}\int_{\Gamma_3}h\Phi^J\widehat{T}^J w_I\,\mathrm{d}\Gamma_3 - \sum_{J=1}^{M}\int_{\Gamma_1}\lambda\left(\frac{\mathrm{d}\Phi^J\widehat{T}^J}{\mathrm{d}x}+\frac{\mathrm{d}\Phi^J\widehat{T}^J}{\mathrm{d}y}\right)n_j w_I\,\mathrm{d}\Gamma = -\int_{\Omega_x}\dot{\Phi}w_I\,\mathrm{d}\Omega_x-\int_{\Gamma_2}qw_I\,\mathrm{d}\Gamma_2+\int_{\Gamma_3}hT_f w_I\,\mathrm{d}\Gamma_3 \quad (23)$$

or

$$\mathbf{K}\cdot\widehat{\mathbf{T}}=\mathbf{F} \quad (24)$$

where M is the total number of nodes in the entire domain Ω, $\widehat{\mathbf{T}}$ the vector for the unknown fictitious nodal values, $\widehat{\mathbf{T}}=[\widehat{T}^1,\widehat{T}^2,\ldots,\widehat{T}^M]$, and $\mathbf{K}$ and $\mathbf{F}$ are the global stiffness matrix and the global vector, respectively, which are defined as

$$K_{IJ}=\int_{\Omega_x}\left(\lambda\frac{\mathrm{d}\Phi^J}{\mathrm{d}x}\frac{\mathrm{d}w_I}{\mathrm{d}x}+\lambda\frac{\mathrm{d}\Phi^J}{\mathrm{d}y}\frac{\mathrm{d}w_I}{\mathrm{d}y}\right)\mathrm{d}\Omega_x + \int_{\Gamma_3}h\Phi^J w_I\,\mathrm{d}\Gamma_3-\int_{\Gamma_1}\lambda\left(\frac{\mathrm{d}\Phi^J}{\mathrm{d}x}+\frac{\mathrm{d}\Phi^J}{\mathrm{d}y}\right)n_j w_I\,\mathrm{d}\Gamma \quad (25)$$

$$F_I=-\int_{\Omega_x}\dot{\Phi}w_I\,\mathrm{d}\Omega_x-\int_{\Gamma_2}qw_I\,\mathrm{d}\Gamma_2+\int_{\Gamma_3}hT_f w_I\,\mathrm{d}\Gamma_3 \quad (26)$$

3. Results of numerical examples and discussion

In this section, MLPG method is applied to compute two-dimensional steady-state heat conduction problems in engineering within irregular domain. The meshless local Petrov–Galerkin (MLPG) method is adopted by using linear basis and quadratic spline weight function, and the transformation method is applied to deal with the essential boundary conditions. A patch case that has analytical solution is solved to illustrate the accuracy and efficiency. Results of two cases in engineering are compared with

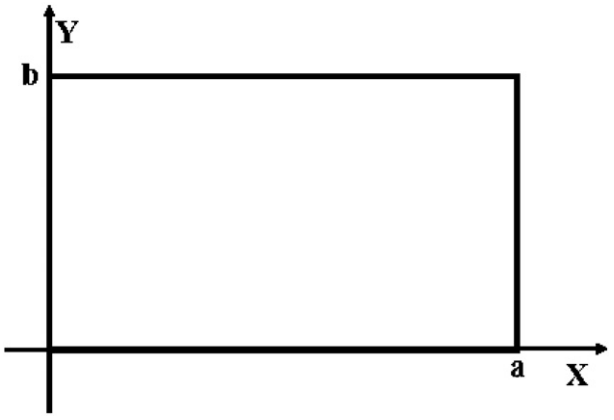

Fig. 3. Problem description for patch test.

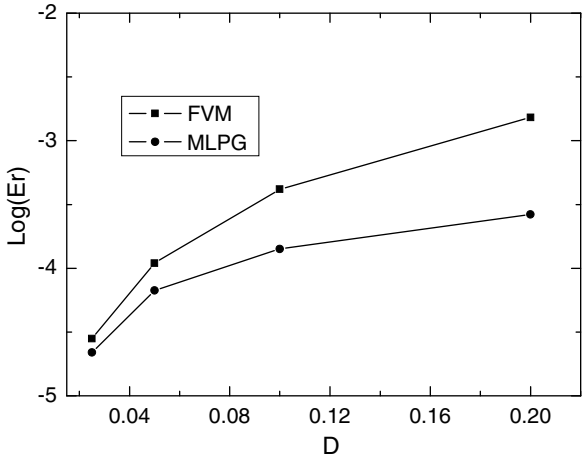

Fig. 4. Relative errors for patch test.

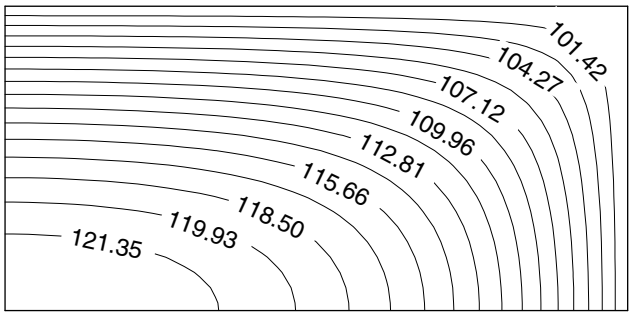

(a) Analytical solution

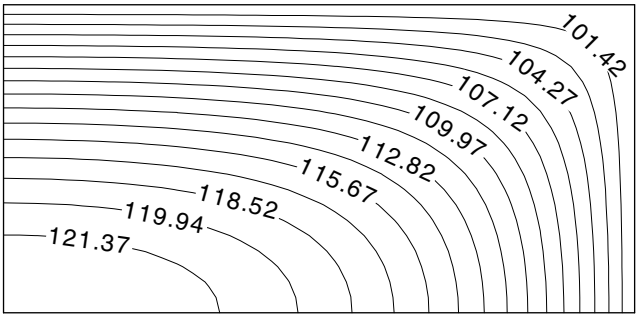

(b) MLPG method

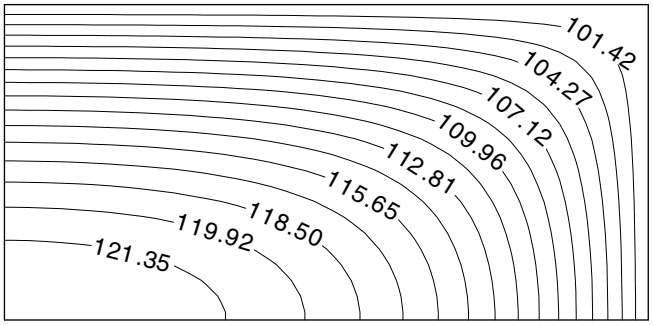

(c) FVM

Fig. 5. Comparison of temperature fields for patch test (°C).

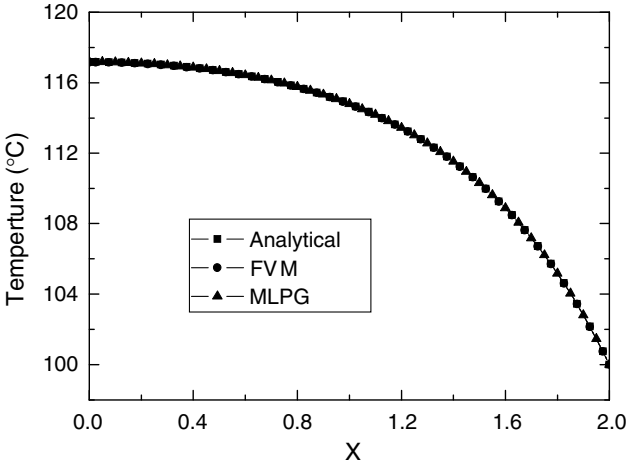

(a) Temperature distribution along y=0.5

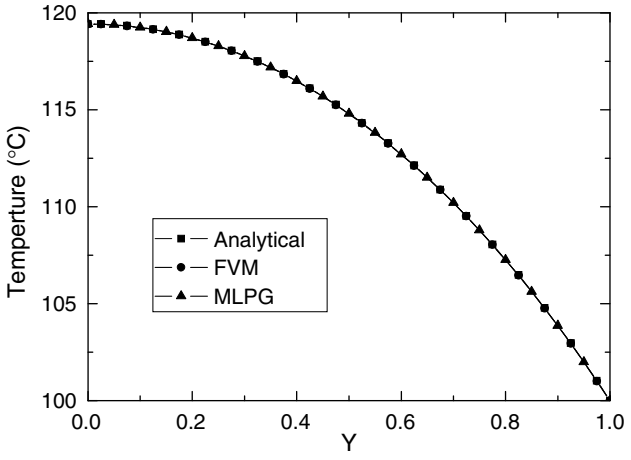

(b) Temperature distribution along x=1.0

Fig. 6. Comparison of temperature distributions for patch test.

the solutions from the finite volume method (FVM) obtained by the commercial CFD package FLUENT 6.3.

3.1. Patch case

A rectangular domain in the dimension 2 m × 1 m is shown in Fig. 3, the bottom and left boundaries are adiabatic, and the upper and right boundaries are maintained at the temperature $T_w = 100$ °C. There exits a uniformly distributed heat source $Q = 50$ W/m^2 in the domain, and

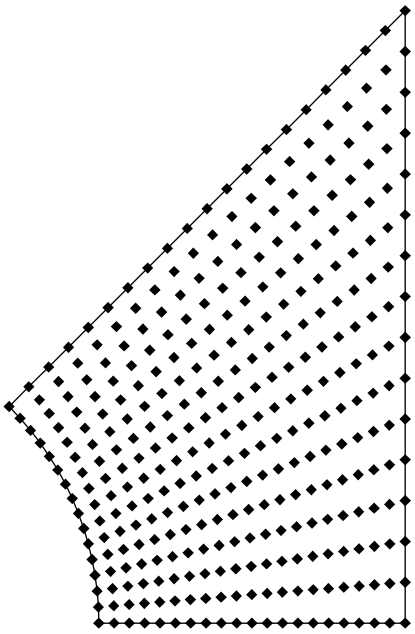

(a) MLPG method

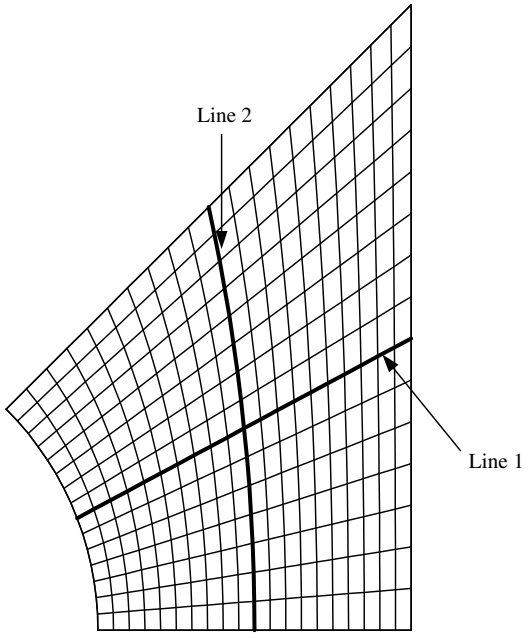

(b) FVM

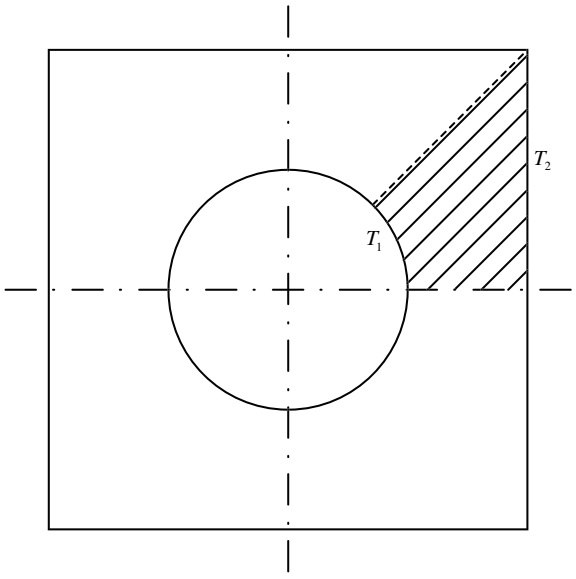

Fig. 7. Physical model and computational domain for insulation of tube transporting vapor.

Fig. 8. Node or mesh distribution for insulation of tube transporting vapor.

the thermal conductivity is $\lambda = 1$ W/(m °C). The analytical solution of this problem is [33]:

$$T(x,y) = \frac{Q}{\lambda\beta_m^3}\sum_{m=1}^{\infty}(-1)^m \frac{2}{a\cosh(\beta_m b)}\cosh(\beta_m y) \times \cos(\beta_m x) + \frac{Q}{2\lambda}(a^2 - x^2) + T_w \quad (27)$$

where $\beta_m = \frac{(2m-1)\pi}{2a}, m = 1, 2, \ldots, N$.

The relative error of the numerical solution is defined as

$$Er = \frac{\sqrt{\sum_{i=1}^{N}(T_i^{\text{num}} - T_i^a)^2}}{\sqrt{\sum_{i=1}^{N}(T_i^a)^2}} \quad (28)$$

where the superscript num denotes numerical results of MLPG method and FVM, a denotes analytical solutions, and N is the total node number.

In the present computation, a uniform node distribution of 41×21 is adopted, and partitions (6×6) are used for the numerical integration; 10 Gauss points are used on each section of Γ; and 6×6 points are used in each local domain Ω_x for numerical quadratures. The relative error is shown in Fig. 4, where the abscissa D is the node distance. It can be seen that MLPG method is more accurate than the finite volume method (FVM). Fig. 5 gives

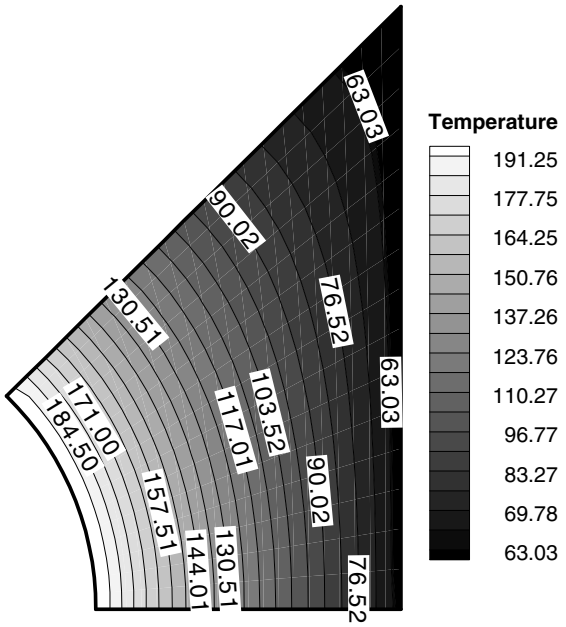

(a) FVM

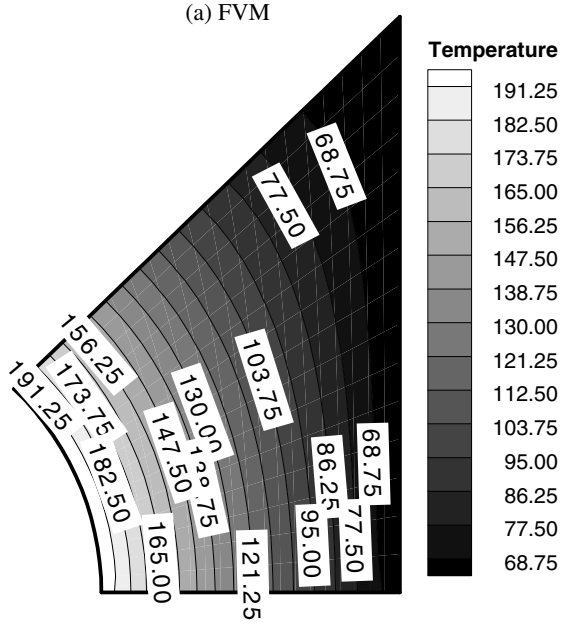

(b) MLPG method

Fig. 9. Comparison of temperature fields for insulation of tube transporting vapor (°C).

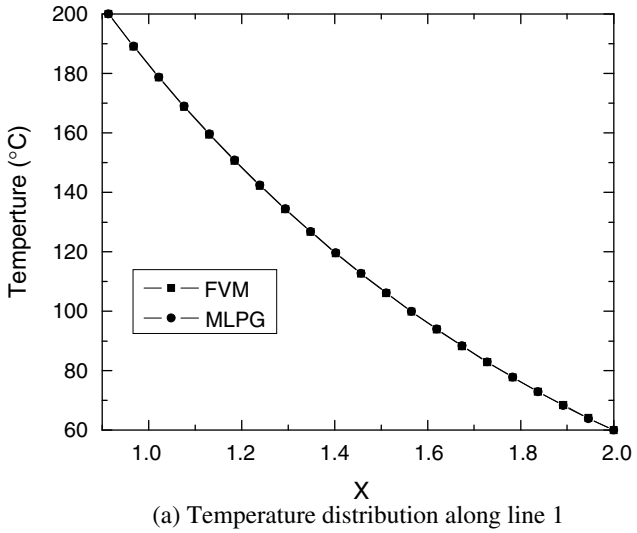

(a) Temperature distribution along line 1

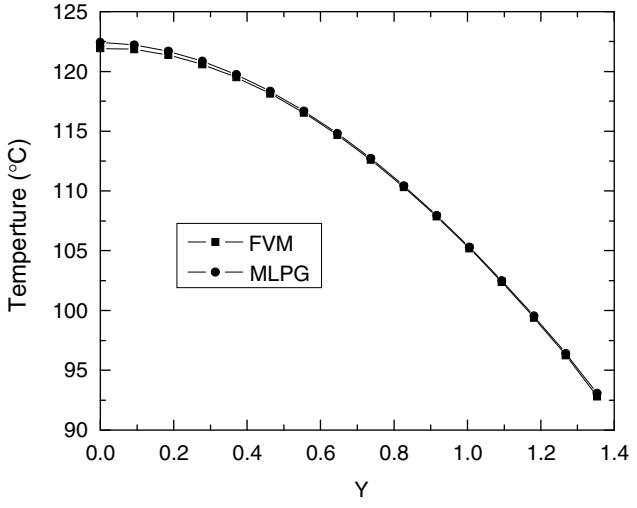

(b) Temperature distribution along line 2

Fig. 10. Comparison of temperature distributions for insulation of tube transporting vapor.

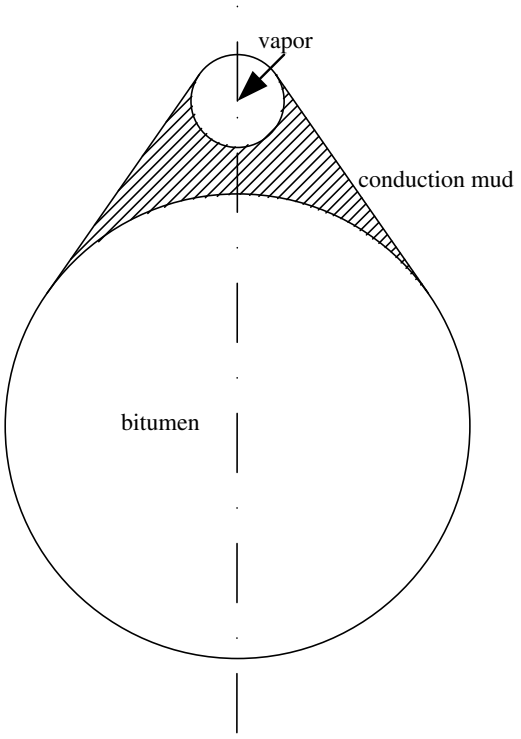

Fig. 11. Physical model and computational domain for insulation of tube transporting bitumen.

predicted temperature fields and Fig. 6 gives predicted temperature distributions along the two centerlines ($x = 0.5$ and $y = 0.5$). From Figs. 5 and 6, we can see that the results from MLPG method and FVM agree very well with the results of analytical solution. This shows that the MLPG method is an efficient and accurate numerical method.

3.2. Insulation of vapor transport tubes

The pipe of vapor transport with a diameter 200 mm is covered by a thermal insulation layer, and which form a square structure of 400 mm × 400 mm, as shown in Fig. 7. Inner surface and outer surface temperature of heat insulation layer is maintained at the temperature $T_1 = 200\ ^\circ\mathrm{C}$ and $T_2 = 60\ ^\circ\mathrm{C}$, respectively. The thermal conductivity of heat insulation layer is $\lambda = 0.1\ \mathrm{W/(m\ ^\circ C)}$. Due to symmetry, only the shadow region is selected as the computational domain.

The selected node distribution of MLPG method and mesh of FVM are shown in Fig. 8. It should be noted that for the comparison purpose, the node distribution in the MLPG is exactly the same as that of FVM. The computational methods are the same as the above case. Figs. 9 and 10 give the predicted temperature fields and temperature distributions along line 1 and line 2 (see Fig. 8b) from the present method and FVM, respectively. The maximum relative error is less than 0.5% for the two curves. The results of the present method are in very good agreement with those obtained by using FVM.

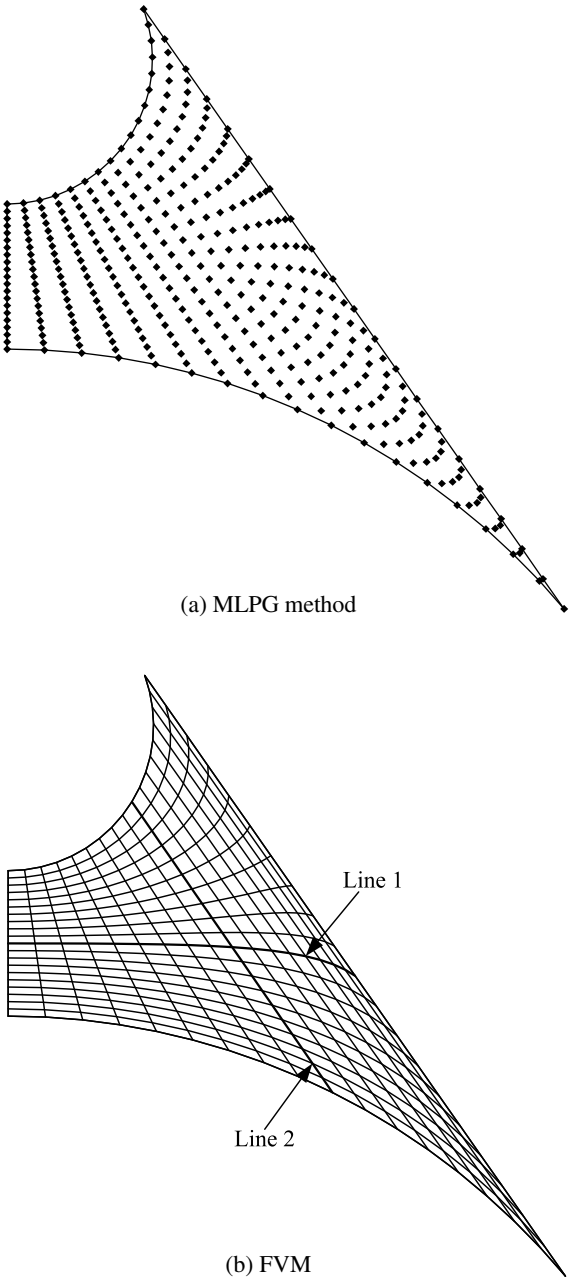

Fig. 12. Node or mesh distribution for insulation of tube transporting bitumen.

3.3. Insulation of tubes for transport of bitumen

In the petrochemical engineering, in order to transport high viscosity material such as petroleum, it often adopts vapor heating system to keep the bitumen at certain temperature, which can efficiently decrease the viscosity of petroleum. The heating system which has steam traced piping or jacketed piping are often adopted. But the efficiency of the stream traced piping is low, and the jacketed piping is not easy to install. In recent years, a kind of new material (conduction mud) which has higher thermal conductivity has been employed. It is filled between a heating pipe and a heated pipe (see Fig. 11), and can significantly enhance

heat transfer between them [34]. In the present case the thermal conductivity of the conduction mud is $\lambda = 10$ W/(m °C), the outer surfaces of two pipes are maintained at the temperature 150 °C and 100 °C, respectively. Due to symmetry, only the right half of shadow domain is numerically modeled.

Node distribution of MLPG method and mesh of FVM are shown in Fig. 12. It should be noted that for the comparison purpose, the node distribution in the MLPG is exactly the same as that of FVM. The computational methods are the same as the above case. Figs. 13 and 14 give

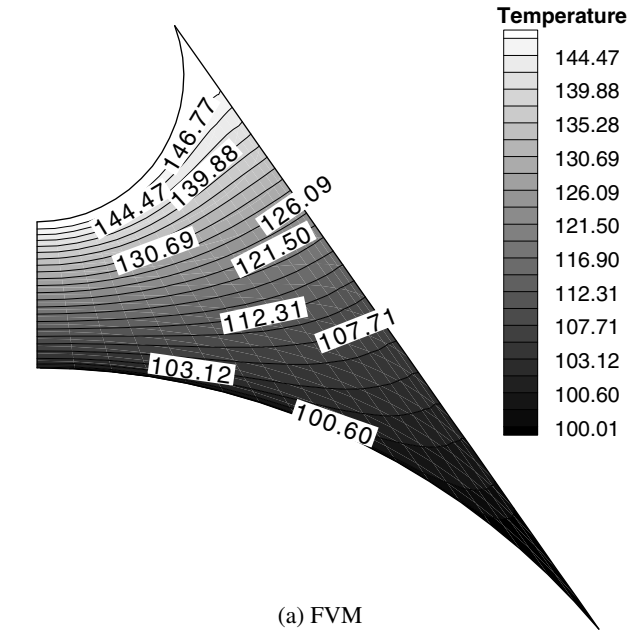

(a) FVM

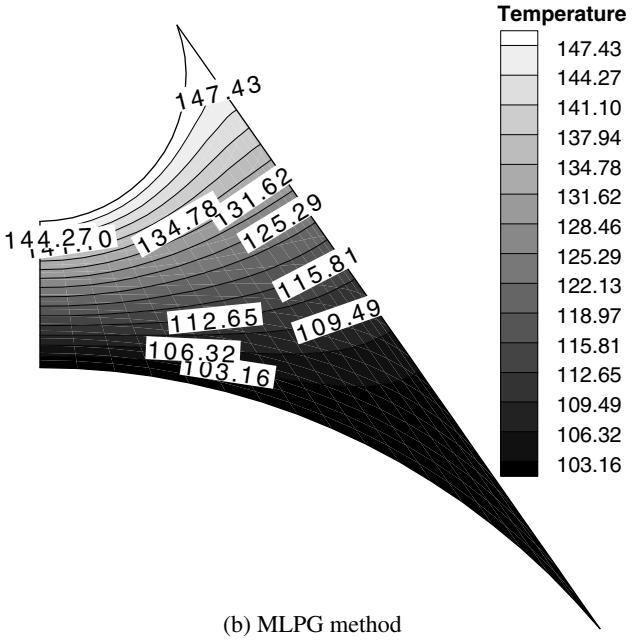

(b) MLPG method

Fig. 13. Comparison of temperature fields for insulation of tube transporting bitumen (°C).

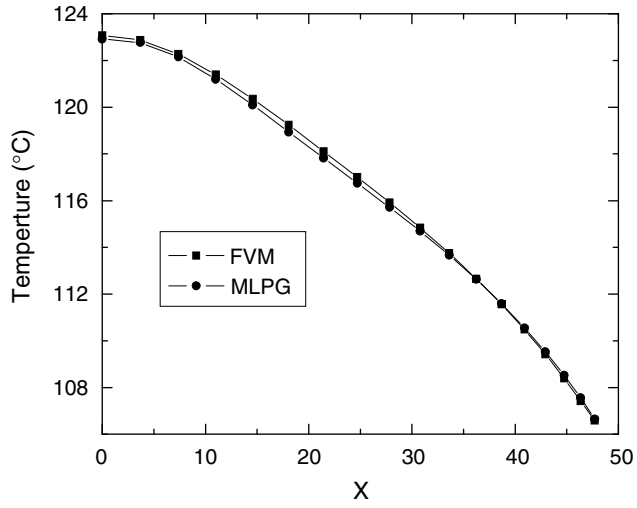

(a) Temperature distribution along line 1

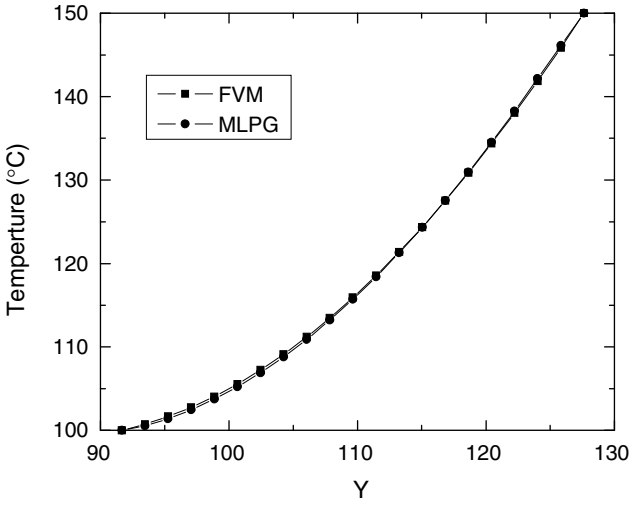

(b) Temperature distribution along line 2

Fig. 14. Comparison of temperature distributions for insulation of tube transporting bitumen.

predicted temperature fields and temperature distributions along line 1and line 2 (see Fig. 12b) of the present method and FVM, respectively. The maximum relative error is less than 0.3% for the two curve. Comparisons of the two results show that they are quite close to each other.

4. Conclusions

In this paper, the meshless method is applied to compute the two-dimensional steady-state heat conduction problems in irregular domain in engineering. The moving least-squares approximation (MLS) is applied to construct the trial functions and the transformation method is employed to deal with the essential boundary condition.

The MLPG results have been compared with the results of FVM using FLUENT 6.3, and the results of MLPG method are in good agreement with those obtained by FVM. From the computational results, it can be seen that

the transformation method can be very effective and accurate to deal with the essential boundary condition of irregular domain. The present study demonstrates that the MLPG method is a high accurate numerical method for problems within irregular domain. The implementation procedure of MLPG method is node based, and it doesn't need background mesh for integration and is a truly meshless method. Thus, it can be expected that MLPG method is very promising in solving engineering heat conduction problems within irregular domains.

Acknowledgement

This work is supported by the National Natural Science Foundation of China (50636050).

References

[1] G.R. Liu, M.B. Liu, Smoothed Particle Hydrodynamics: A Meshfree Particle Method, World Scientific Publishing Co. Pte. Ltd., Singapore, 2003.
[2] L.B. Lucy, A numerical approach to testing of the fission hypothesis, Astron. J. 8 (1977) 1013–1024.
[3] J.J. Monaghan, Smoothed particle hydrodynamics, Annu. Rev. Astron. Astrophys 30 (1992) 543–574.
[4] B. Nayroles, G. Touzot, P. Villon, The diffuse approximations, C.R. Acad. Sci. Paris Sér. II 313 (1991) 133–138.
[5] B. Nayroles, G. Touzot, P. Villon, The diffuse element method, C.R. Acad. Sci. Paris Sér. II 313 (1991) 293–296.
[6] T. Belytschko, Y.Y. Lu, L. Gu, Element-free Galerkin methods, Int. J. Numer. Methods Eng. 37 (1994) 229–256.
[7] W.K. Liu, S. Jun, Y.F. Zhang, Reproducing kernel particle methods, Int. J. Numer. Methods fluid 20 (1995) 1081–1106.
[8] E. Onate, S. Idelsohn, O. Zienkiewicz, R.L. Taylor, A finite point method in computational mechanics application to convective transport and fluid flow, Int. J. Numer. Methods Eng. 39 (1995) 3839–3866.
[9] S.N. Atluri, T. Zhu, A new meshless local Petrov–Galerkin (MLPG) approach in computational mechanics, Comput. Mech. 24 (1998) 348–372.
[10] S.N. Atluri, T. Zhu, A new meshless local Petrov–Galerkin (MLPG) approach to nonlinear problems in computer modeling and simulation, Comput. Model. Simulat. Eng. 3 (1998) 196–197.
[11] S.N. Atluri, S.P. Shen, The Meshless Local Petrov–Galerkin (MLPG) Method, Tech Science Press, Encino USA, 2002.
[12] H. Sadat, S. Couturier, Performance and accuracy of a meshless method for laminar natural convection, Numer. Heat Transfer, Part B 37 (2000) 455–467.
[13] T. Sophy, H. Sadat, C. Prax, A meshless formulation for three-dimensional lammiar natural convection, Numer. Heat Transfer, Part B 41 (2002) 433–445.
[14] I.V. Singh, P.K. Jain, Parallel meshless EFG solution for fluid flow problems, Numer. Heat Transfer, Part B 48 (2005) 45–66.
[15] Y.L. Wu, G.R. Liu, Y.T. Gu, Application of meshless local Petrov–Galerkin (MLPG) approach to simulation of incompressible flow, Numer. Heat Transfer, Part B 48 (2005) 459–475.
[16] P.W. Cleary, J.J. Monaghan, Conduction modeling using smoothed particle hydrodynamics, J. Comput. Phys 148 (1999) 27–264.
[17] J.K. Chen, J.E. Beraun, T.C. Carney, A corrective smoothed particle method for boundary value problems in heat conduction, Int. J. Numer. Meth. Eng. 46 (1999) 231–252.
[18] A. Singh, I.V. Singh, R. Prakash, Numerical solution of temperature-dependent thermal conductivity problems using a meshless method, Numer. Heat Transfer, Part A 50 (2006) 125–145.
[19] I.V. Singh, K. Sandeep, R. Prakash, Heat transfer analysis of two-dimensional fins using meshless element-free Galerkin method, Numer. Heat Transfer A 44 (2003) 73–84.
[20] I.V. Singh, K. Sandeep, R. Prakash, The element free Galerkin method in three-dimensional steady state heat conduction, Int. J. Comput. Eng. Sci. 3 (2002) 291–303.
[21] I.V. Singh, R. Prakash, The numerical solution of three-dimensional transient heat conduction problems using element free Galerkin method, Int. J. Heat Tech. 21 (2003) 73–80.
[22] I.V. Singh, A numerical solution of composite heat transfer problems using meshless method, Int. J. Heat Mass Transfer 47 (2004) 2123–2138.
[23] Y. Liu, X. Zhang, M.W. Liu, A meshless method based on least-squares approach for steady-and unsteady state heat conduction problems, Numer. Heat Transfer 47 (2005) 257–275.
[24] J.Y. Tan, L.H. Liu, B.X. Li, Least-squares collocation meshless approach for coupled radiative and conductive heat transfer, Numer. Heat Transfer, Part B 49 (2006) 179–195.
[25] H. Sadat, N. Dubus, L. Gbahoue, T. Sophy, On the solution of heterogeneous heat conduction problems by a diffuse approximation meshless method, Numer. Heat Transfer, Part B 50 (2006) 491–498.
[26] L.F. Qian, R.C. Batra, Three dimensional transient heat conduction in a functionally graded thick plate with a high order plate theory and a meshless local Petrov Galerkin method, Comput. Mech. 35 (2005) 214–226.
[27] J. Sladek, V. Sladek, S.N. Atluri, Meshless local Petrov–Galerkin method for heat conduction problem in an anisotropic medium, CMES: Comput. Model. Eng. Sci. 6 (3) (2004) 309–318.
[28] J. Sladek, V. Sladek, Ch. Hellmich, J. Eberhardsteiner, Heat conduction analysis of 3-D axisymmetric and anisotropic FCM bodies by meshless local Petrov–Galerkin method, Comput. Mech. 39 (2007) 323–333.
[29] Y.Y. Lu, T. Belytschko, L. Gu, A new implementation of the element free Galerkin method, Comput. Methods Appl. Mech. Eng. 113 (1994) 397–414.
[30] G.R. Liu, X.L. Chen, J.N. Reddy, Buckling of symmetrically laminated composite plates using the element-free Galerkin method, Int. J. Struct. Stabil. Dyn. 2 (2002) 281–294.
[31] S.N. Atluri, H. Kim, J.Y. Cho, A critical assessment of the truly meshless local Petrov–Galerkin(MLPG) and local boundary integral equation (LBIE) methods, Comput. Mech. 24 (1999) 348–372.
[32] R.G. Liu, Y.T. Gu, An Introduction to Meshree Methods and their Programming, Springer-Verlag Press, Berlin, 2005.
[33] M. Necati Ozisik, Heat conduction, Wiley, New York, 1980.
[34] C.R. Chen, Y.D. Hu, C.Y. Zhao, Q.W. Wang, W.Q. Tao, Numerical study on heat transfer characteristic of conduction mud, J. Eng. Thermophys. 22 (1) (2001) 101–103 (in Chinese).